Critical Transitions in the Biofabrication of Abalone Shells and Flat Pearls

Charlotte M. Zaremba,[†] Angela M. Belcher,[†,‡,∥] Monika Fritz,[‡,§,∥,@] Youli Li,[⊥,∥] Stephen Mann,[#] Paul K. Hansma,[§,∥] Daniel E. Morse,[‡,∥] James S. Speck,[⊥,∥] and Galen D. Stucky*[,†,⊥,∥]

Department of Chemistry, Marine Biotechnology Center and Department of Biological Sciences, Department of Physics, Department of Materials, and Materials Research Laboratory, University of California, Santa Barbara, California 93106, and School of Chemistry, University of Bath, Bath BA2 7AY, United Kingdom

Received July 18, 1995. Revised Manuscript Received October 6, 1995[⊗]

Analyses of biopolymer/calcium carbonate composites grown on inorganic abiotic substrates implanted between the shell and the shell-secreting epithelium of live red abalones (*Haliotis rufescens*) provide detailed spatial and temporal data on the in vivo assembly process that generates the shell. X-ray diffraction and scanning electron microscopy analyses of the growth of these *flat pearl* composites reveal that biomineralization is initiated by the deposition of an organic sheet on the implanted substrate, followed by the growth of a calcite layer with preferred {10.4} orientation and, finally, by the growth of nacreous aragonite. The calcite layer is structurally similar to the green organic/calcite heterolayer of native shell nacre. It comprises 0.2−2.0-μm-diameter elongated crystallites of typical geological habits in various aggregate arrangements. The shell also contains an external layer of (00.1)-oriented prismatic calcite, which is deposited on one edge of a flat pearl and has a morphology similar to that of the {10.4}-oriented calcite layer. The transition from {10.4}-oriented calcite to aragonite in both the shell and the flat pearl is abrupt. In vitro calcium carbonate growth experiments reveal that a similar calcite-to-aragonite transition is induced by the addition of soluble proteins isolated from the aragonitic nacre. The growth of flat pearls is highly sensitive to physical and chemical properties of the abiotic substrate. Either roughened or hydrophobic substrates result in abnormal arrangements of the basal calcite layer, which are corrected for by a reinitiation of the biomineralization process, beginning with the deposition of an organic sheet. Insertion of flat pearls as substrates, however, results in continued nacre growth without the deposition of an organic sheet and a calcite layer.

Introduction

Biominerals are formed by a wide variety of organisms and perform a diverse array of functions. Yet all biominerals can be classified as either *biologically induced* or *biologically controlled*, depending on the extent of biological regulation of their formation.[1] Biologically controlled biominerals are formed by plants and animals.[1] These materials are organic/inorganic composites that often exhibit order at the nanometer level and often comprise structurally pure inorganic phases. In biologically controlled biomineralization, crystal nucleation, phase, morphology, and growth dynamics are directed on a space−time basis by biopolymers and/or biomolecular processes. The resulting materials frequently contain well-ordered arrays of monodisperse subunits (Figure 1). When crystalline, the subunits often have preferred orientations and unusual shapes and sizes. Because this range of control over mineral growth is desirable for materials engineering applications, there is much interest in understanding the mechanisms of biologically controlled biomineralization.[2,3]

In our studies of mollusc and bivalve biomineralization,[4−6] our interest is in understanding all of the mineralization processes, including larval shell growth and metamorphosis into the juvenile phase[7] as well as adult shell development.[8] At each of these life stages, the shell has an elaborate, but synergistic, composite

† Department of Chemistry.
‡ Marine Biotechnology Center and Department of Biological Sciences.
§ Department of Physics.
⊥ Department of Materials.
∥ Materials Research Laboratory.
University of Bath.
@ Present address: MPI für Biochemie, Molekulare Strukturbiologie, 82152 Martinsried, Germany.
* To whom correspondence should be addressed.
⊗ Abstract published in *Advance ACS Abstracts,* November 15, 1995.

(1) Lowenstam, H. A. *Science* **1981**, *211*, 1126.
(2) Berman, A.; Hanson, J.; Leiserowitz, L.; Koetzle, T. F.; Weiner, S.; Addadi, L. *Science*, **1993**, *259*, 776.
(3) Birchall, J. D. In *Biomineralization: Chemical and Biochemical Perspectives*, Mann, S., Webb, J., Williams, R. J. P., Eds.; VCH: Weinheim, 1989; p 491.
(4) Fritz, M.; Belcher, A. M.; Radmacher, M.; Walters, D. A.; Hansma, P. K.; Stucky, G. D.; Morse, D. E.; Mann, S. *Nature* **1994,** *371*, 49.
(5) Manne, S.; Zaremba, C. M.; Giles, R.; Huggins, L.; Walters, D. A.; Belcher, A.; Morse, D. E.; Stucky, G. D.; Didymus, J. M.; Mann, S.; Hansma, P. K. *Proc. R. Soc. London B* **1994**, *256*, 17.
(6) Giles, R.; Manne, S.; Zaremba, C. M.; Belcher, A.; Mann, S.; Morse, D. E.; Stucky, G. D.; Hansma, P. K. *Mater. Res. Soc. Symp. Proc.* **1994**, *332*, 413.
(7) Cariolou, M. A.; Morse, D. E. *J. Comp. Physiol. B* **1988**, *157*, 717.
(8) Morse, D. E.; Cariolou, M. A.; Stucky, G. D.; Zaremba, C. M.; Hansma, P. K. *Mater. Res. Soc. Symp. Proc.* **1993**, *292*, 59.

0897-4756/96/2808-0679$12.00/0

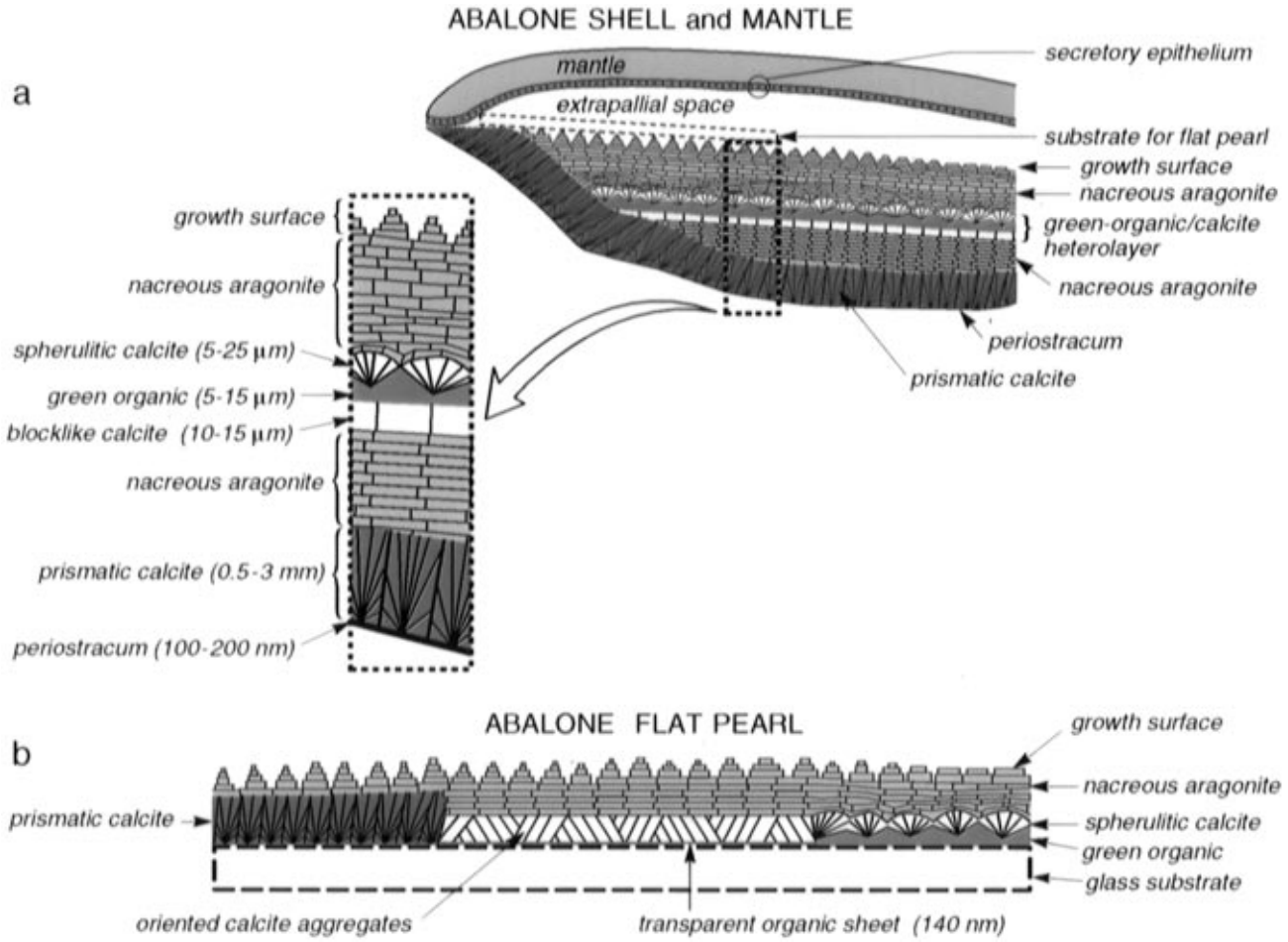

Figure 1. (a) Schematic (not drawn to scale) of a vertical section of the outer edge of the shell and mantle of a red abalone (*Haliotis rufescens*) with an enlargement indicating thickness dimensions of the shell structures. The size of the extrapallial space is exaggerated for clarity. (b) Schematic of a flat pearl grown on a glass coverslip (not drawn to scale). In both schematics, the secretory epithelium of the mantle contacts the biomineral growth surface from above, and the nacre is shown as pink to signify its iridescence.

organization of organic and inorganic components. One therefore needs to characterize the various organic−organic, organic−inorganic, and inorganic−inorganic phase transitions as they occur.

Understanding the formation process of molluscan nacre is particularly important since, through the strategic incorporation of 1−5 wt % organic matter in an organic/aragonite composite,[9] nacre achieves a fracture toughness that is $\sim 3 \times 10^3$ times greater than that of pure aragonite ($CaCO_3$).[10] The organic phase is clearly a critical component of both the atomic and composite assembly of nacre, which is accomplished with high degrees of both local (Å)- and long-range (μm) order.[9] The long-range order results in beautiful optical interference colors as well as in fracture toughness.

Red abalone nacre contains tabular single crystals of aragonite 0.4 μm thick and 5−10 μm wide. These crystals, termed *tablets*, are arranged in flat sheets parallel to the shell surface and in columnar stacks normal to the shell surface, with interdigitation of the tablets at stack edges (Figure 1). All tablets are oriented with the aragonitic (orthorhombic) *c* axis normal to their faces.[5,11] This crystal habit differs from that of aragonite formed in seawater, which is typically elongated along the *c* axis.[12] The individual stacks of tablets have been reported to be approximately single crystalline,[5,11,13,14] although, in bulk, nacre exhibits random orientation in the plane of the shell surface.[11] Nacre grows in conical stacks of tablets[11,15] within a stack of thin (10−50 nm),[16] porous, continuous organic sheets,[15,17] termed the *organic matrix*. Nacre is deposited on the prismatic calcite outer layer of the shell.

Successful in vitro application of the crystal growth techniques that produce ordered biominerals such as red abalone nacre will require thorough mechanistic and structural knowledge. Previous studies have addressed the nucleation of oriented crystals on ordered organic monolayers[18] and the morphology and crystallography of different shell layers.[5,15,16,19] There have been relatively few comprehensive studies[20] of the ultrastructure,

(9) Weiner, S. *CRC Crit. Rev. Biochem.* **1986**, *20*, 365.
(10) Currey, J. D. *Proc. Roy. Soc. London B* **1977**, *196*, 443. Jackson, A. P.; Vincent, J. F. V. *J. Mater. Sci.* **1990**, *25*, 3173.
(11) Wise, S. W. *Ecologae Geol. Helv.* **1970**, *63*, 775.
(12) Bathurst, R. C. *Developments in Sedimentology*, 2nd ed.; Elsevier: New York, 1975; Vol. 12.
(13) Wilbur, K. M.; Saleuddin, A. S. M. In *The Mollusca*; Wilbur, K. M., Ed.; Academic: New York, 1983; Vol. 4, p 235.
(14) Sarikaya, M.; Gunnison, K. E.; Yasrebi, M.; Aksay, I. A. *Mater. Res. Soc. Symp. Proc.* **1990**, *174*, 109.
(15) Nakahara, H.; Bevelander, G.; Kakei, M. *Venus* **1982**, *41*, 33.
(16) Sarikaya, M.; Aksay, I. A. In *Results and Problems in Cell Differentiation*; Case, S. T., Ed.; Springer-Verlag: Berlin, 1992; Vol. 19, p 1.
(17) Nakahara, H. In *Mechanisms and Phylogeny of Mineralization in Biological Systems*; Suga, S., Nakahara, H., Kaigi, N. G., Eds.; Springer-Verlag: Tokyo, 1991; p 343.
(18) Heywood, B. R.; Mann, S. *Chem. Mater.* **1994**, *6*, 311. Mann, S.; Heywood, B. R.; Rajam, S.; Walker, J. B. A. *J. Phys. D. Appl. Phys.* **1991**, *24*, 154.

crystallography, growth sequence and transitions, and interrelationships of all components of the shell. Comprehensive knowledge of the shell may help explain puzzling aspects of nacre growth. These include the role of nucleation, the origin of each nacreous stack, the growth of monodisperse single crystals (tablets and tablet stacks) at controlled rates, and the determinants of both structural phase and uniformity in tablet thickness. The nucleation and structure-directing processes that give rise to calcite morphologies in the shell are equally unresolved. It seems likely that a full understanding of nacre growth will require knowledge of the interphase transition chemistry and structure of the entire shell.

We recently demonstrated a method for spatially and temporally monitoring in vivo the entire shell-formation process, beginning with the deposition of an organic sheet and proceeding through the various structures and growth transitions that comprise the biomineralization of gastropod molluscs.[4] Here we describe the application of this methodology, by studying the in vivo growth of *flat pearls* to obtain detailed structural information about calcite and aragonite growth transitions in the shell of the red abalone (*Haliotis rufescens*; marine gastropod mollusc).

Background and Approach

Adult red abalone shells (Figure 1a) can reach 30 cm in diameter. Shell precursors are secreted by epithelial cells of the *mantle*, a thin secretory tissue lining the inner surface of the shell (Figure 1a). The shell grows from aqueous solution in the *extrapallial space*, a thin compartment between the mantle and the inner surface of the shell (Figure 1a). Three layers are deposited sequentially from the exterior to the interior of the shell. In order of deposition, these layers include (1) a brown 100−200-nm-thick[15] organic sheet called the *periostracum*, (2) a red 0.5−3-mm-thick calcite layer called *prismatic calcite*, and (3) an iridescent 0−12-mm-thick aragonite layer called *nacreous aragonite*, or *nacre*, which thickens throughout life. An additional green organic/calcite heterolayer is interspersed through the nacre at irregular intervals. This layer was characterized recently by other researchers.[21,22]

The growth processes forming these shell layers can be monitored by examining abiotic substrates inserted between the growing edge of the shell and the mantle of live red abalones (Figure 1).[4] The iridescent flat pearls that are ultimately produced on these substrates contain differentiated regions that are faithful biochemical, crystallographic, and ultrastructural reproductions of components of the native adult shell.[4] For example, all four layers of the native shell (described above) are deposited sequentially during flat pearl growth. Previous researchers have studied early mineral deposition on glass coverslips[23−26] and other abiotic substrates[25] inserted between the mantle and the shell of marine bivalves. However, in these cases, the initial organic sheet[27] and the earliest mineral deposition[23,26] were of interest. The progression of mineral deposition to nacre was not reported. Typically, the sequential progression to nacre has been studied by removing a marginal portion of the shell of a live mollusc and allowing it to be regenerated.[28,29] This process, termed *shell regeneration*, is studied by sacrificing animals at intervals and analyzing the regenerated shell regions. Shell regeneration begins with the deposition of an organic sheet.

We have studied substrates implanted between the mantle and the shell of live molluscs because the resulting flat-pearl-growth samples are easy to both generate and analyze. In general, the consequences of chemical and physical modification of the growth media can be quickly observed. The abiotic substrate can be removed and reinserted at any time during the biomineralization process. Furthermore, the effects of chemically and physically different substrates on flat pearl growth can reveal the adaptability and critical components of the biomineralization system. Thus, the analysis of flat pearl growth results in spatial and temporal resolution of the mechanisms by which the animal generates shell structures, transitions between organic and/or inorganic phases, and other growth features.

Experimental Procedure

Live adult red abalones were maintained at 14 °C in fresh, flowing, filtered seawater, with saturation feeding of fresh kelp (*Macrocystis pyrifera*). Substrates were inserted between the mantle and the inner surface of the shell's peripheral edge (Figure 1).[4] Substrates included 0.2-mm-thick, 18-mm-diameter circular glass coverslips (Fisher) and molybdenite (MoS_2) cleaved along the (00.1) plane into flakes ~0.4 mm thick and 4−9 mm wide. Roughened glass substrates were prepared by etching glass coverslips in 49% hydrofluoric acid for 10 min followed by thorough rinsing with water.

Growing flat pearls were removed after 1−30 days and stored briefly in sterile, filtered seawater (0.2-μm filter). As noted above, growing flat pearls could be reinserted in animals. Prior to analysis, they were rinsed in 0.04 *m* NH_4HCO_3 buffer (3 g/L) and blotted dry with a paper tissue. Growing flat pearls were imaged with a Nikon optical microscope with both reflected and transmitted light between crossed polarizers to identify 2−4-mm-wide regions of uniform mineral coverage. These regions were analyzed by X-ray diffraction and scanning electron microscopy (SEM). Vertical sections for SEM were prepared by fracturing.

X-ray diffraction studies were carried out on either a Philips 4-circle diffractometer or a Scintag powder diffractometer. On the 4-circle diffractometer, X-ray measurements were made using grazing-incidence double-mirror incident optics (Ni-coated glass) with horizontal and vertical slits. The diffracted beam optics included a soller slit assembly and a flat graphite monochromator. SEM was carried out on a JEOL JSM-6300F instrument equipped with a cold cathode field-emission source. Uncoated samples were examined with beam energies of 3−3.5 kV (resolution ~25 Å at these voltages). Stereoscopic SEM pairs were made by collecting double images with a 7° relative inclination. Energy-dispersive X-ray analyses (EDXA) were conducted using a JEOL 840A scanning electron microscope equipped with a Tracor Northern Series II X-ray analyzer (15

(19) Mutvei, H. In *Origin, Evolution, and Modern Aspects of Biomineralization in Plants and Animals*; Crick, R. E., Ed.; Plenum: New York, 1991; p 137.
(20) Addadi, L.; Weiner, S. In *Biomineralization: Chemical and Biochemical Perspectives*; Mann, S.; Webb, J.; Williams, R. J. P., Eds.; VCH: Weinheim, 1989; p 133.
(21) Erasmus, J.; Cook, P. A.; Sweijd, N. *J. Shellfish Res.* **1994**, *13*, 493.
(22) Shepherd, S. A.; Avalos-Borja, M.; Ortiz Quintanilla, M. *Aust. J. Mar. Freshwater Res.* **1995**, *46*, 607.
(23) Wada, K. *Bull. Natl. Pearl Res. Lab.* **1961**, *7*, 703.
(24) Bevelander, G.; Benzer, P. *Biol. Bull.* **1948**, *94*, 176.
(25) Watabe, N.; Wilbur, K. M. *Nature* **1960**, *88*, 334.
(26) Wada, K. *Bull. Natl. Pearl Res. Lab.* **1964**, *9*, 1087.
(27) Wada, K. *Bull. Jpn. Soc. Sci. Fisheries* **1964**, *4*, 993.
(28) Watabe, N. In *The Mollusca*; Wilbur, K. M., Ed.; Academic: New York, 1983; Vol. 4, p 235.
(29) Suzuki, S. *Chishitsugaku Zasshi (J. Geol. Soc. Jpn.)* **1983**, *89*, 433.

kV). Samples for EDXA were mounted with silver paint on aluminum mounts and sputter-coated with carbon.

Feigl staining[30] was used to distinguish aragonite from calcite in native-shell and flat-pearl samples. Staining was conducted by immersion in Feigl's solution[30] of $MnSO_4$, $AgSO_4$, and NaOH overnight at room temperature, followed by thorough rinsing with water and imaging by reflection optical microscopy. Aragonite is stained black; calcite remains colorless. Mineral-specific, water-soluble, polyanionic proteins from the aragonite and calcite phases of the native shell were isolated and separated as described previously.[4] Optical microscopy was conducted with thin (10−15 μm) vertical sections of green organic/calcite heterolayers from native-shell nacre. The sections were prepared by embedding thin nacre pieces (∼0.3 mm) in LR white resin and microtoming with a diamond knife.

Results

A substrate with iridescent nacre deposited on a preceding organic sheet and calcite layer is termed a *flat pearl*. The transplantation of a flat pearl from one organism to another results in no interruption in nacre production evident in vertical fracture sections examined by SEM. The implantation of glass or molybdenite substrates, however, results in the deposition of an organic sheet followed by calcite on regions of the substrate apposed to the nacreous aragonite of the shell (Figure 1). We previously described this response as a *default* to reinitiation of the biomineralization sequence.[4] Prismatic calcite is deposited on a region of the substrate apposed to the prismatic calcite growth surface of the shell.

{10.4}-Oriented Calcite. Two types of organic sheets, transparent and green, are deposited on the region of the glass coverslip substrate apposed to nacre (Figure 1). The transparent organic sheet is deposited first, in a central 5−15-mm-diameter region of the substrate. It is ∼140 nm thick, as shown in Figure 3b. Within 1 day of implantation, a 4-μm-thick layer of colorless calcite is deposited on the transparent organic sheet (Figure 3b). Within 2 days of implantation, the green organic sheet is deposited in a 1−10-mm-wide band on the circumference of the substrate. The green sheet grows to a thickness of 5−15 μm (Figure 5a). In general, calcite structures on the transparent sheet grow vertically more quickly (∼5.0 μm/day) than those on the green sheet (∼1.2 μm/day) and are overgrown with nacre sooner than those on the green sheet.

On both the transparent and green organic sheets, the smallest calcite structures are 0.2−2.0-μm-diameter elongated crystallites, which nucleate on {10.4} faces, yet grow along their *c* axes (Figure 2). The nucleation orientation of these crystallites [{10.4}] is thus different from the growth orientation [(00.1)]. In the calcite crystal structure, these planes are relatively inclined by 45°. In Figure 2a, {10.4} planes can be observed at the bases of prism-shaped crystallites.

The elongated crystallites exhibit a wide range of morphologies, as shown in Figure 2, all of which are consistent with geological forms of calcite.[12,31−33] Crystallite diameter and length increase with duration of implantation. Along the *c* axis, the crystallites often have either horizontal (Figure 2b,d) or diagonal (Figure 2c) striations. The latter correspond to {10.4} planes of calcite. Also along the *c* axis, crystal morphology is often poorly defined with rough lateral edges (Figure 2b,c). At early growth stages (1−6 days), the elongated crystallites commonly exhibit scalenohedron morphologies in which six scalene triangular faces meet at a point and are related by 3-fold rotational symmetry (Figure 2b,c). Expression of the lateral crystal faces increases with prolonged growth until, after increased implantation time (∼2 weeks), many crystallites exhibit hexagonal prism shapes (Figure 2a,d). In another morphological variation, the crystallites appear to comprise stacks of 50-nm-thick *c*-axis-face plates with hexagonal lateral edges (Figure 2d). Morphological variation in the elongated crystallites may depend on the extent of spatial confinement, the dissolved $[Ca^{2+}]/[CO_3^{2-}]$ ratio, and the rapidity and duration of crystal growth.[32,34]

Calcite Crystallite Aggregates on the Transparent Organic Sheet. On the transparent organic sheet, the elongated crystallites are densely packed into oriented, irregularly shaped, 30−150-μm-wide polycrystalline aggregates that behave as aligned single crystals when imaged by transmission optical microscopy between crossed polarizers (Figure 3c). Each polycrystalline aggregate has a specific in-plane orientation (Figure 3c). Nucleation is initiated at discrete sites such that the aggregate density is ∼350 aggregates/mm^{-2}. Within 1 day of implantation, the aggregates grow laterally to form an almost continuous layer (<12 μm interaggregate gaps). Within each oriented aggregate, the crystallites are identically inclined ∼45° from the plane of the substrate surface (Figure 3b,d). This inclination results from the crystallites growing in the [00.1] direction after having nucleated from the {10.4} plane, as discussed above. Roughly uniform inclination angles over the entire layer of polycrystalline aggregates results in high {10.4} orientation, as shown in the pole figure of transparent-organic-sheet calcite on a 3-day growing flat pearl (Figure 3a). The {10.4} peak is centered about the flat pearl surface normal with a full width at half maximum (fwhm) of only 3.1°.

By 6 days after implantation, the polycrystalline aggregates often have rounded, dome-shaped upper surfaces observable by both SEM and transmission optical microscopy between crossed polarizers. After a 5−15-μm-thick layer of oriented polycrystalline aggregates has been deposited, it is often overgrown with spherulitic calcite aggregates. Calcite on the transparent organic sheet achieves a total thickness of 10−50 μm before being overgrown with nacre.

Calcite Crystallite Aggregates on the Green Organic Sheet. On the green organic sheet, aggregates of elongated crystallites are less well aligned. They undergo nonuniform, windmill-like extinctions when rotated during transmission optical microscopy between crossed polarizers. A pole figure of green-organic-sheet calcite on an 8-day growing flat pearl indicates preferred {10.4} orientation with the {10.4} peak centered about the flat pearl surface normal (Figure 4a). However, there is misalignment about the ⟨10.4⟩ direction, as revealed by the fwhm of 21.2°. The degree of {10.4} alignment of green-organic-sheet calcite increases with flat pearl implantation time.

(30) Feigl, A.; Anger, V. *Spot Tests in Inorganic Analysis*; Elsevier: Amsterdam, 1972; p 542.
(31) Dana, J. D. *Mineralogy*, 17th ed.; John Wiley and Sons: New York, 1959.
(32) Given, R. K.; Wilkinson, B. H. *J. Sed. Petrol.* **1985**, *55*, 109.
(33) Grigor'ev, D. P. *Ontogeny of Minerals*; Israel Program for Scientific Translations: Jerusalem, 1965.
(34) Lahann, R. W. *J. Sed. Petrol.* **1978**, *48*, 337.

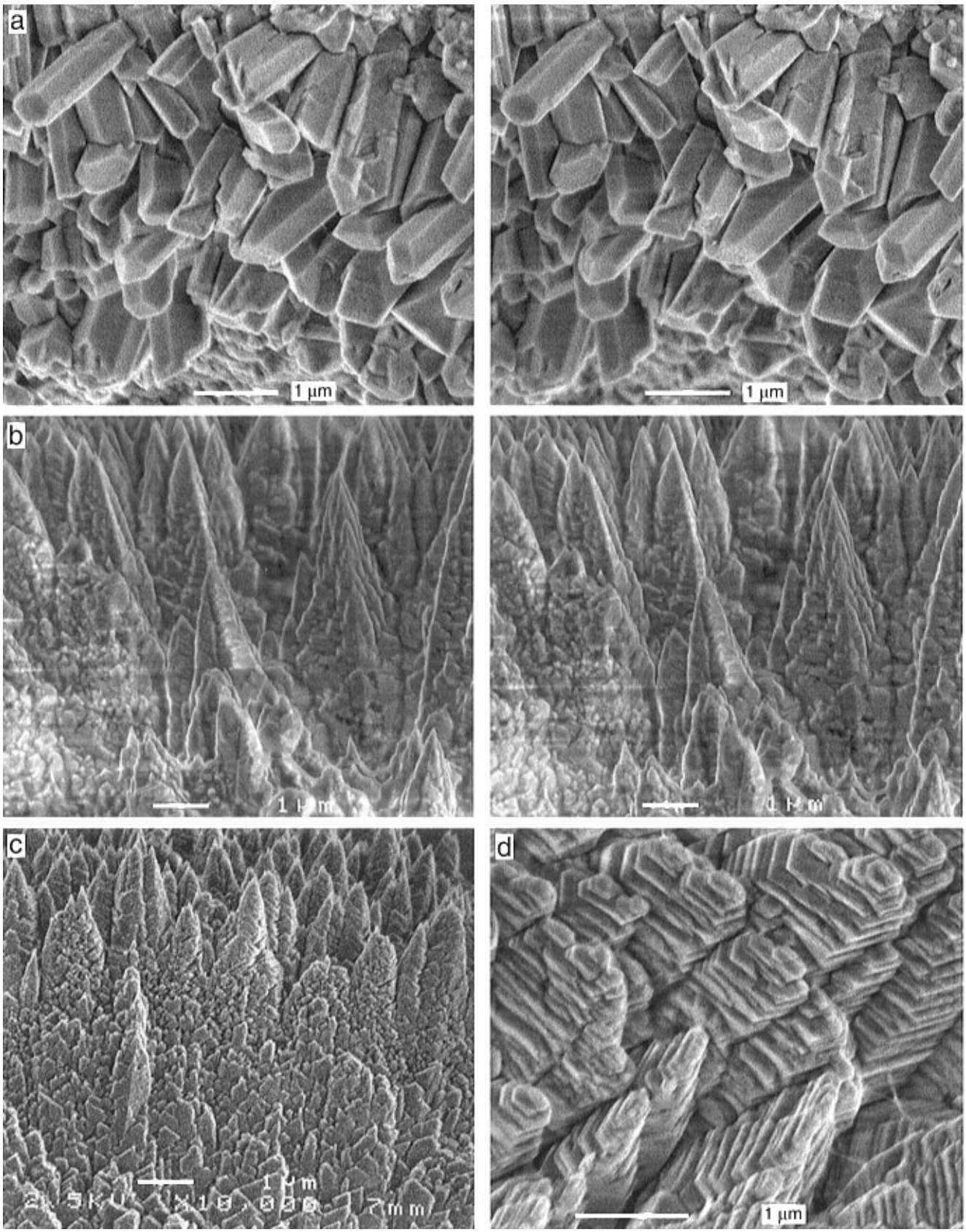

Figure 2. (a) Stereopair SEM images (vertical section) of hexagonal prism calcite crystallites grown on the transparent organic sheet of a flat pearl. Note the rhombohedral faces at the bases of the crystallites. (b) Stereopair SEM images and (c) a single SEM image (both in plan view) of scalenohedron calcite crystallites grown on the transparent organic sheet of a 6-day growing flat pearl. In (b), the crystallites exhibit striations oriented normal to the growth axes; the horizontal streaks on the left side of the image are due to sample charging. In (c), the striations are oblique to the growth axes, and correspond to {10.4} calcite faces. (d) SEM image (plane of substrate tilted 7°) of calcite crystallites on the green organic sheet of a 14-day growing flat pearl, which exhibit *c*-axis-face layering.

On the green organic sheet, elongated crystallites sometimes aggregate in vertical or tilted rows that resemble blades. However, in a more common arrangement, spherulitic crystallite aggregates nucleate on the

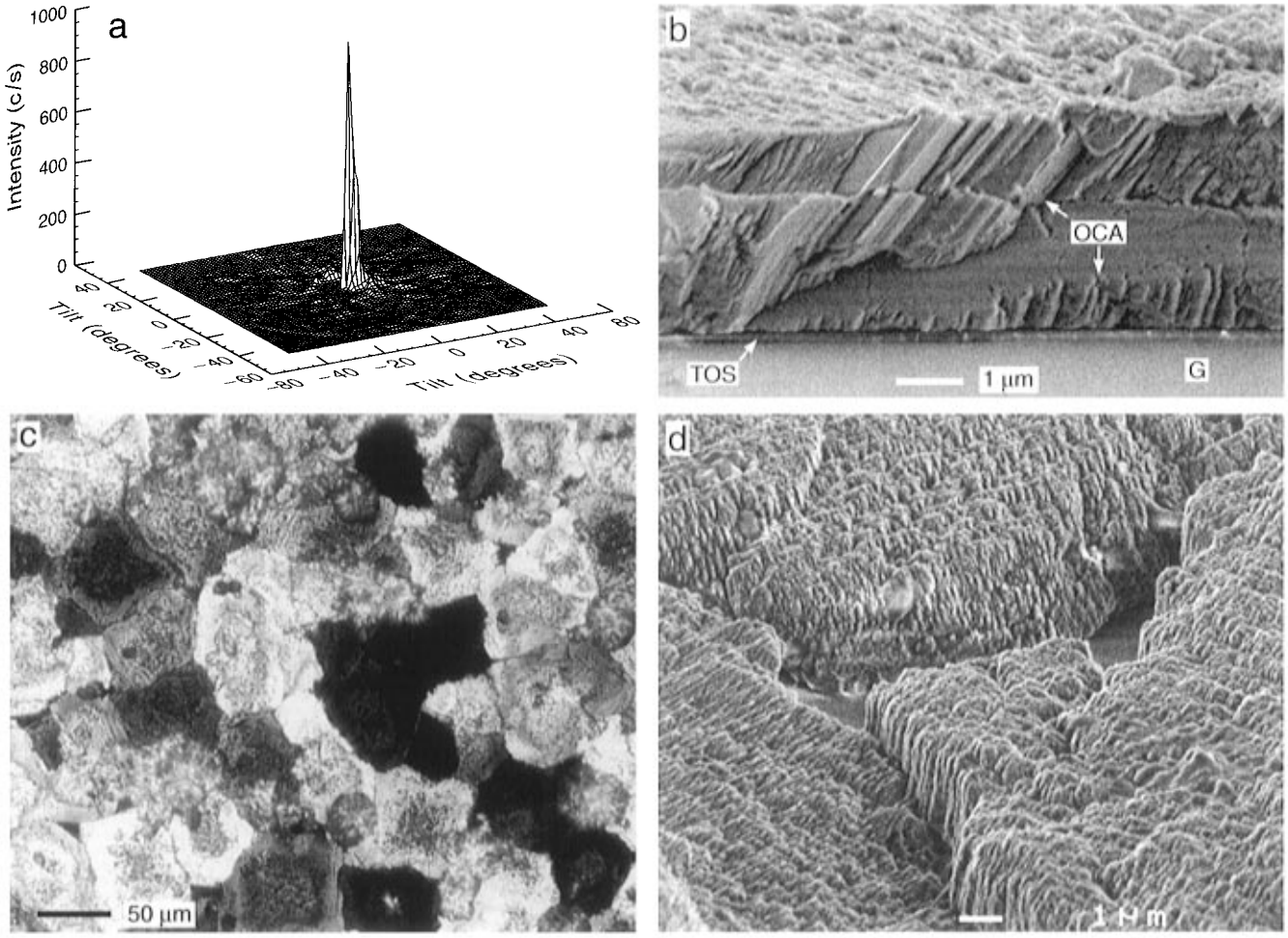

Figure 3. (a) {10.4} pole figure of transparent-organic-sheet calcite on a 3-day growing flat pearl. (b) SEM image of a vertical section of *transparent-organic-sheet* (TOS) calcite on a 1-day growing flat pearl. Growth direction is bottom to top. Note the two differently *oriented* polycrystalline *calcite aggregates* (OCA); G, *glass*. (c) Transmission optical microscopy image with crossed polarizers of transparent-organic-sheet calcite of a 2-day growing flat pearl. (d) SEM image (plane of substrate tilted 30°) of three oriented polycrystalline aggregates in transparent-organic-sheet calcite on a 1-day growing flat pearl. The aggregates are distinguishable by the unique in-plane orientations of their constituent crystallites.

green sheet at discrete sites spaced by 25−100 μm (Figures 4b and 5a) such that the nucleation density is ~140 spherulites/mm^{-2}. The spherulites are often flattened and irregularly shaped. They begin growth as disklike polycrystalline aggregates in which the elongated crystallites are more vertically oriented at the center, increasingly tilted towards the edges, and more horizontally oriented at the rim (Figure 4b). Calcite aggregates on the green organic sheet achieve a total thickness of 10−20 μm before being overgrown with nacre (Figure 5a).

The green organic sheet comprises two sublayers, as shown in Figure 5a. The layer apposed to the substrate, termed *organic layer 1* (OL1), is 2−5 μm thick and densely granular, comprising 100-nm-diameter granules. OL1 is separated from the second organic layer, termed *organic layer 2* (OL2), by a nearly horizontal interface. OL2 is 2−20 μm thick, depending on its position beneath the hemispheric spherulites. OL2 charges heavily in the SEM, exhibiting the high-contrast regions observed in Figure 5a. OL2 has a smoother textural appearance than OL1 and has been observed to contain a spongy, interconnected network of 30-nm-diameter fibers. The interface between OL2 and the undersides of the calcite spherulites is physically weak. In SEM images of flat pearl vertical sections, this interface is frequently manifest as a crack that zigzags along a horizontal plane between the two layers, tracing the hemispheric undersides of the spherulites (Figure 5a).

Both sublayers of the green organic sheet are traversed by winding, mostly vertical filaments ~150 nm wide and 8−10 μm long, which are spaced by 5−15 μm (Figure 5a). In the SEM, the brightness of these filaments (uncoated) often contrasts with the darkness of the surrounding material (Figure 5a). This is suggestive of a difference in composition. EDXA of spots on these filaments indicates that they contain variable amounts of calcium, depending on filament diameter. On average, however, the filaments contain 4−5 times as much calcium as the surrounding (organic) material. Therefore, we speculate that the filaments may be calcium carbonate structures growing through the green organic sheet.

Green Organic/Calcite Heterolayers in Native Shell Nacre. Green organic/calcite heterolayers from native shell nacre are structurally similar to green-organic-sheet regions of flat pearls. Vertical sections of native shell heterolayers are shown schematically in Figure 1a and by SEM in Figure 5b. Feigl staining, SEM, EDXA, and Raman microprobe spectroscopy[35] of

(35) Belcher, A. M.; Wu, X. H.; Christensen, R. J.; Hansma, P. K.; Stucky, G. D.; Morse, D. E. *Nature*, in press.

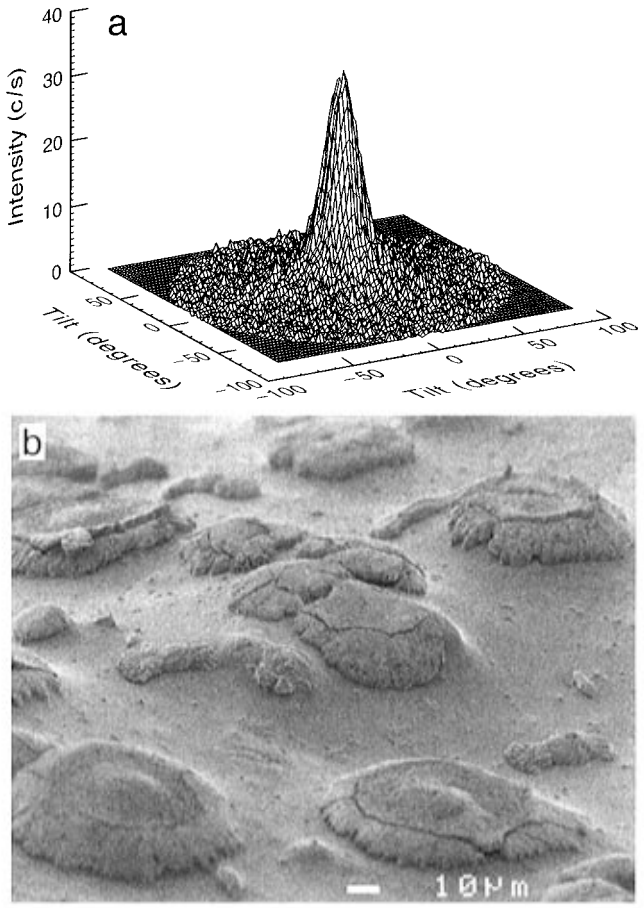

Figure 4. (a) {10.4} pole figure of green-organic-sheet calcite on an 8-day growing flat pearl. (b) SEM image (plane of substrate tilted 73°) of green-organic-sheet calcite on a 6-day growing flat pearl with disklike polycrystalline aggregates.

vertical sections of these layers indicate that, in order of deposition, a calcite sublayer, an organic sublayer, and a second calcite sublayer intervene between the interruption in and reinitiation of nacre growth (Figures 1a and 5b). Each sublayer is 5−25 μm thick. Transmission optical microscopy of thin sections of the heterolayer reveals that the calcite sublayers are colorless and that the organic sublayer is green. The first calcite sublayer, termed *blocklike calcite*, is 10−15 μm thick. It contains 10−20-μm-wide oriented subunits that undergo unique extinctions when rotated during transmission optical microscopy between crossed polarizers. Blocklike calcite contains vertically oriented grooves and cleavage planes, shown in Figure 5b. The most prominent of these are spaced by 5−10 μm and often coincide with boundaries between stacks of tablets in the underlying nacre. Because of these vertical features, blocklike calcite often resembles an abnormally thick layer of nacreous tablets in SEM of vertical sections.

The organic sublayer deposited on blocklike calcite is 5−15 μm thick (Figures 1a and 5b). The interface between these sublayers is abrupt, straight, and nearly horizontal with respect to the shell surface (Figure 5b). EDXA reveals that the organic sublayer generally has a low calcium content (~20 times lower than that of calcite). In addition to being green, this sublayer is structurally similar to the green organic sheet of flat pearls in that it contains the two organic layers OL1 and OL2, and high-calcium filaments (Figure 5b). In the native shell heterolayer, however, the filaments

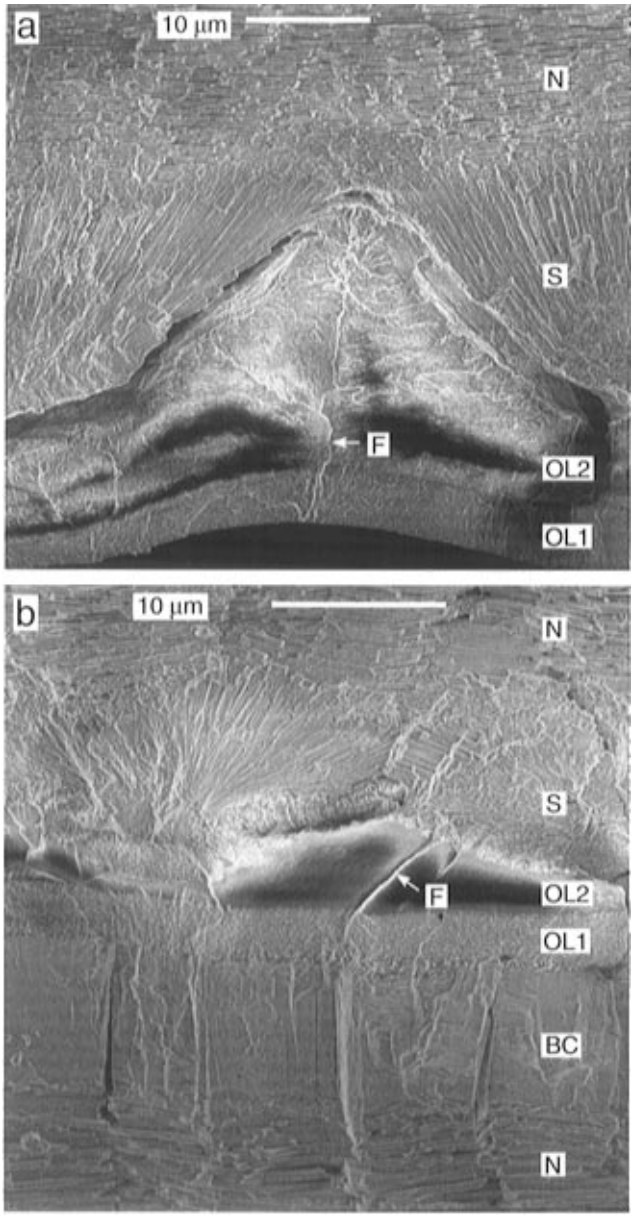

Figure 5. SEM images of vertical sections of (a) a green organic sheet and spherulitic calcite layer of a flat pearl and (b) a green organic/calcite heterolayer of native shell nacre. The direction of growth in both images is bottom to top. BC, blocklike calcite; F, filament; N, nacreous aragonite; OL1, organic layer 1; OL2, organic layer 2; S, spherulitic calcite. The dark regions of OL2 are due to charging from the electron beam. In (a), the lower surface of the organic sheet is curved due to buckling during drying.

extend from the first to the second calcite sublayer and are usually initiated at the tops of prominent vertical cleavage planes in the blocklike calcite (Figure 5b). The filaments are 150 nm in diameter, 7−13 μm long, and spaced by 2−11 μm.

The organic sublayer is overgrown by a 5−25-μm-thick layer of calcite spherulites spaced 15−50 μm apart (Figure 5b), which is structurally similar to the calcite layer grown on the green organic sheet of flat pearls. The interface between OL2 and the spherulitic calcite sublayer of native shell heterolayers resembles the analogous interface in flat pearls in that it is poorly defined and often physically weak, cracking in a zigzag pattern along the hemispheric undersides of the spherulites during fracture. Aragonitic nacre resumes growth on the spherulitic calcite sublayer (see below).

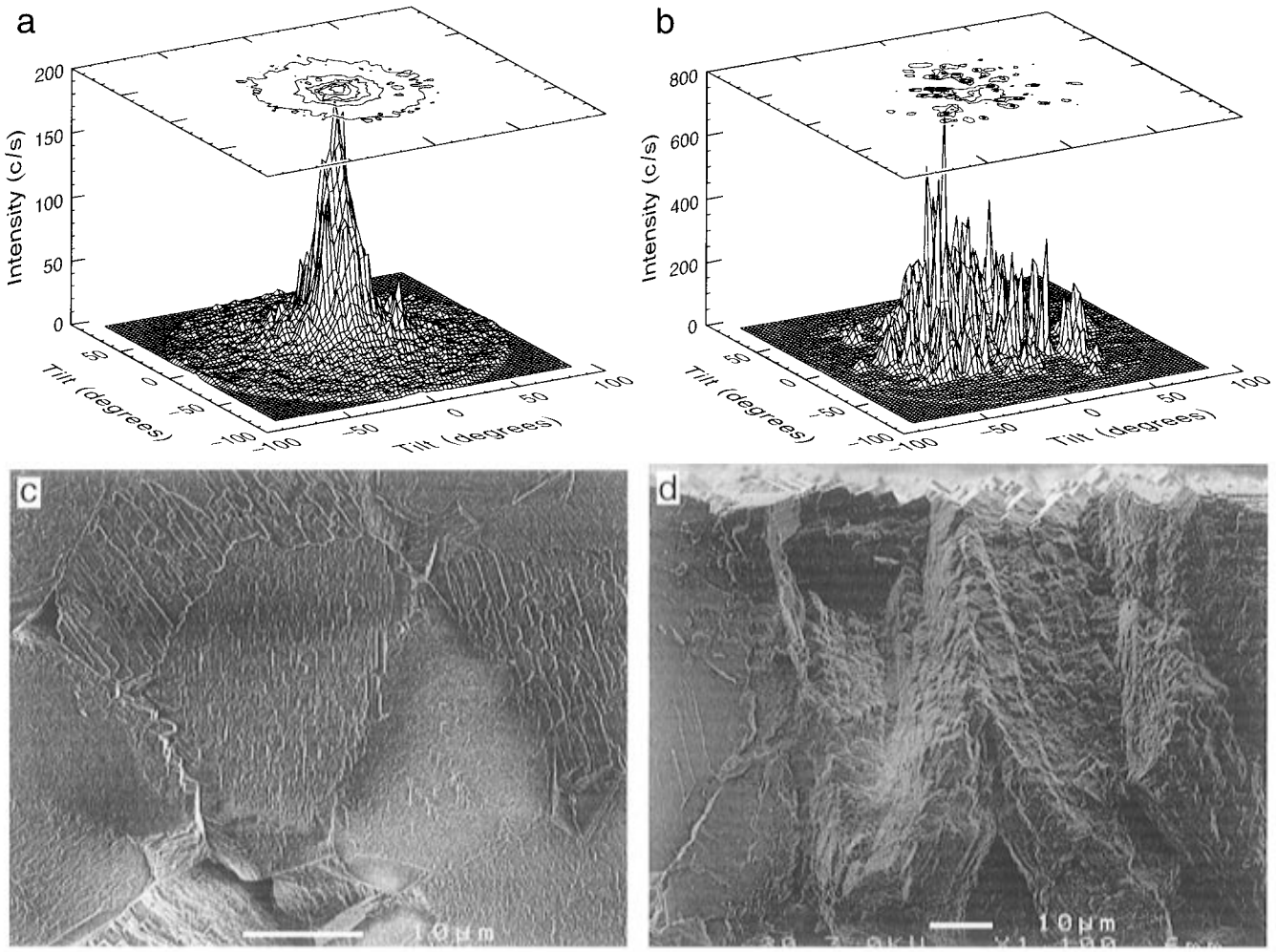

Figure 6. (a) (00.6) and (b) {10.4} pole figures of prismatic calcite on a 4-day growing flat pearl. SEM images of (c) a plan view and (d) a vertical section of prismatic calcite on a 6-day growing flat pearl. In (d), the growth direction is bottom to top.

(00.1)-Oriented Prismatic Calcite. Prismatic calcite grows in a 1−3-mm-wide *growth band* on the margin of the shell's inner lip (Figure 1a). It is also deposited in a 1−3-mm-wide band on one edge of a flat pearl whose substrate is positioned partially above the prismatic calcite growth band of the shell (Figure 1). Prismatic calcite has been reported to comprise prism-shaped aggregates of uniformly oriented, 0.1−0.2-μm-diameter acicular crystallites,[19] termed *polycrystalline prisms*. The red color of prismatic calcite is derived from metabolites.[36]

In the native shell, the crystallographic texture of prismatic calcite is difficult to characterize. The growth surface is naturally curved and the bulk material fractures irregularly. Growing flat pearls implanted for less than 13 days, however, have prismatic calcite growth surfaces that are flat and, therefore, are highly amenable to textural analysis by X-ray diffraction. The (00.6) pole figure of such a surface reveals preferred (00.l) orientation (Figure 6a). The calcite (00.6) reflection is centered about the flat pearl surface normal with a broad fwhm of 24.6° (Figure 6a). A pole figure of the calcite {10.4} reflection is highly spotty in nature, as shown in Figure 6b. This spottiness is indicative of coarse grain size. If we assume that we can associate each peak in the {10.4} pole figure with one polycrystalline prism, then an approximate prism diameter can be calculated. The X-ray beam illuminates ~3 mm^2 of the sample, and we count ~40 {10.4} peaks in the pole figure. This corresponds to an approximate lateral grain size of 160 μm. This value agrees with Mutvei's SEM measurements of 100−200 μm prism diameters.[19]

Plan-view SEM and transmission optical microscopy of prismatic calcite in 4−13-day growing flat pearls reveal that each polycrystalline prism is distinguishable by the unique and uniform shapes and parallel alignment of its 0.2−1.0-μm-wide constituent crystallites (Figure 6c). The lateral boundaries of the polycrystalline prisms have irregular shapes. The prisms are 30−100 μm in diameter at the proximal edge of the prismatic calcite growth band and 50−200 μm in diameter at the distal edge. This size difference indicates that the prisms expand laterally with vertical growth. When rotated during transmission optical microscopy between crossed polarizers, irregularly shaped prism subunits of $^1/_5$−$^2/_3$ times the prism areas (20−100-μm-wide regions) undergo uniform extinction at a time. This result contrasts with Mutvei's observation that each prism undergoes complete extinction.[19] The difference between these results may be attributed to the early stage in development of the prisms on growing flat pearls, which have not yet grown vertically and obliquely into more complete alignment.

SEM of vertical sections of flat pearl prismatic calcite indicates that the polycrystalline prisms originate as spherulitic cones from discrete nucleation sites (Figure 6d, bottom) and have rhombohedral growth surfaces (Figure 6d, top). Vertical sections of prismatic calcite

(36) Comfort, A. *Biol. Rev. Cambridge Philos. Soc.* **1951**, *26*, 285.

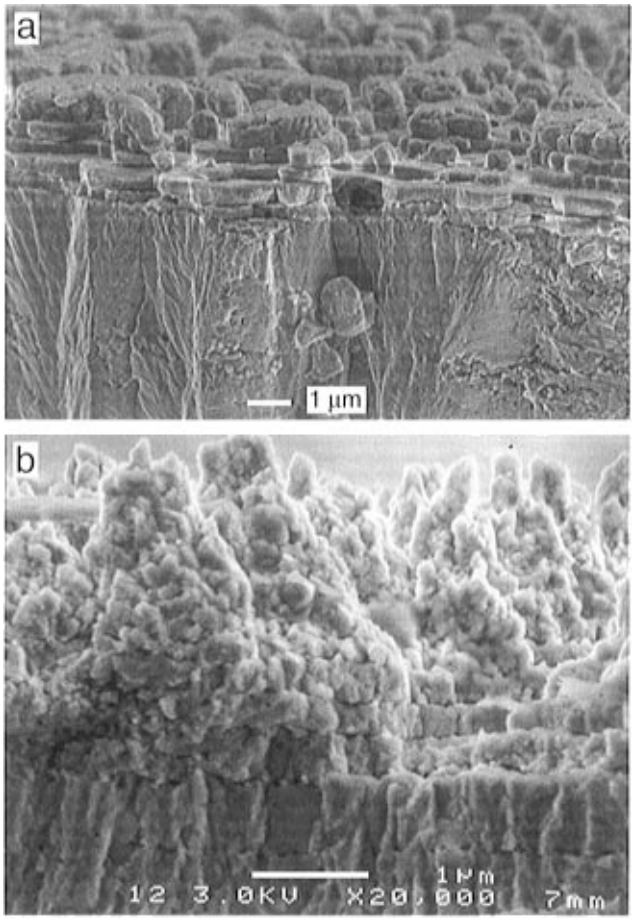

Figure 7. SEM images of vertical sections of (a) a sharp calcite-to-nacreous-aragonite transition region in a 14-day flat pearl and (b) a granular aragonite transition from calcite to nacre in a 6-day growing flat pearl. In both images, the growth direction is bottom to top.

in both flat pearls and the native shell reveal two types of fracture surfaces. These include a rough surface containing obliquely oriented crystallites and a featureless surface characteristic of crystallographic cleavage (Figure 6d). Both types of fracture surfaces can be found in a single polycrystalline prism (Figure 6d).

In growing flat pearls, the growth surfaces of both {10.4}-oriented and (00.1)-oriented calcite structures are periodically coated with ~200-nm-thick horizontal organic sheets, as Mutvei observed in native-shell prismatic calcite.[19] Due to the intermittent deposition of these sheets, some growing flat pearls are coated while others remain uncoated. In both SEM and optical microscopy, the sheets appear as smooth films which obscure morphological details. Therefore, we predominantly imaged samples that lacked these coatings.

Transitions to Nacre. In flat pearl vertical sections, {10.4}-oriented calcite is separated from aragonitic nacre by either a sharp ultrastructural transition (Figures 1b and 7a) or a transition region comprising aragonite with a granular crystal habit (Figure 7b) and random crystallographic orientation (X-ray data not shown). However, in either case there is a surprisingly abrupt transition from a calcite to an aragonite phase. Both types of transition regions can be found in close (10 μm) lateral proximity. SEM data do not show organic sheet structures at these regions. While the calcite-to-aragonite transition is generally sharply defined within narrow (1 μm) lateral regions, calcite crystals often penetrate vertically into the aragonite

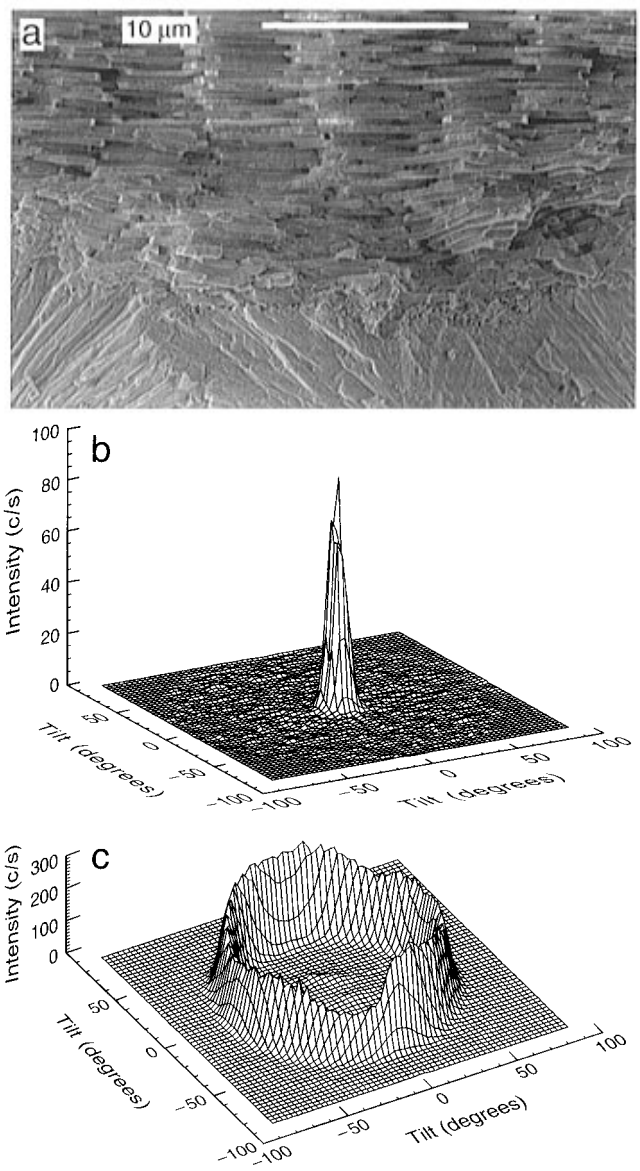

Figure 8. (a) SEM image of a vertical section of a flat pearl showing a transition from spherulitic calcite to nacre. The growth direction is bottom to top. (b) (002) pole figure and (c) (111) pole figure of flat pearl nacreous aragonite.

region in a way that seems to preclude the presence of a continuous, horizontal, organic sheet structure, certainly one such as OL1 or OL2. Transmission electron microscopy data have shown, however, that the aragonite tablets of nacre are each surrounded by a thin organic sheath.[15−17] For this reason, the presence of biopolymers between the calcite and aragonite phases cannot be excluded.

The granular aragonite transition region is preceded by horizontal disruptions in the calcite structure (Figure 7b, bottom). Next, submicron-sized granular crystals of aragonite are deposited in conical stacks (Figure 7b, top). After deposition of a 0.3−4.0-μm thickness of granular crystals, whole tablets are deposited in conical growth stacks. The sharp calcite-to-nacreous-aragonite transition seems to occur on calcite surfaces that are flat and that have a structural similarity to nacre. For example, in Figure 7a, packets of vertical calcite crystallites have lateral dimensions comparable to those of the overlying aragonite nacreous tablets (5−10 μm).

As shown in Figures 1, 5b, and 8a, the calcite surfaces on which nacre grows often have micron-scale rough-

ness. The final nacre ultrastructure, however, is always strikingly flat. Nacre deposition responds to rough calcite surfaces by growing around protrusions and by making graded adjustments in tablet thickness. The first type of adaptation is manifest where groups of calcite crystallites 1−5 μm wide and up to 10 μm high protrude into nacre. The second type of adaptation is manifest in nacre grown on the undulating surface of a spherulitic calcite layer, which exhibits 2−10 μm variations in height (Figures 5 and 8a). This unevenness is corrected for within 20−30 nacreous layers (8−12 μm) by variations in tablet thickness such that tablets in spherulite valleys are thicker than those on spherulite crests (Figure 8a).

In addition to being flat, the final nacreous aragonite product is highly oriented. (002) pole figures of flat pearl nacre indicate a strong preferred (001) orientation with a fwhm of 12°, as shown in Figure 8b. Within the plane of the nacreous layers, however, crystallographic orientation is random, as demonstrated by the (111) pole figure in Figure 8c.

Adaptations to Different Substrates. The multilayer biomineralization process that culminates in nacre growth corrects for both physical and chemical irregularities in growth surfaces. The implantation of roughened glass coverslips results in either regions of local disorder or disruptions in the basal calcite layer grown on the transparent organic sheet. Therefore, on regions of the basal calcite layer with lateral extents of 20 to hundreds of microns, an abnormally thick (15−30 μm) organic layer is deposited (Figure 9a). The interface between these layers is unusually weak and separates to yield 6−12-μm-thick gaps, as shown in Figure 9a. The organic layer is coated with a spherulitic calcite layer followed by nacre.

The implantation of molybdenite substrates results in the growth of calcite crystallite aggregates with a wide range of growth-direction orientations relative to the substrate surface (Figure 9b, bottom). This variation may result from the deposition of nucleating organic sheets in orientations different from that of the substrate surface. The abnormal deposition may arise because the hydrophilic surfaces of the organic sheets do not wet the hydrophobic surface of the molybdenite substrate. Another possibility is that the organic sheets self-assemble with their most hydrophobic components in closest contact with the molybdenite surface. Such behavior has been observed and characterized in our laboratories by in situ atomic force microscopy studies of the organization of amphiphilic molecules on the (00.1) face of single-crystal molybdenite.[37]

Because the organic nucleating sheets are extensively disorganized and convoluted on the molybdenite surface, isolated 10−25-μm-wide aggregates of calcite crystallites grow haphazardly in various growth directions. The crystallites often exhibit *c*-axis-face layering, as in Figure 2d. An unusual example of this type of crystal growth is shown in Figure 9c. Perhaps in response to texture recognition of the variously oriented calcite aggregates,[4] a correction sequence consisting of a 10−20-μm-thick organic layer and a 10-μm-thick spherulitic calcite layer with the usual growth orientation is deposited, followed by nacre (middle to top of Figure 9b).

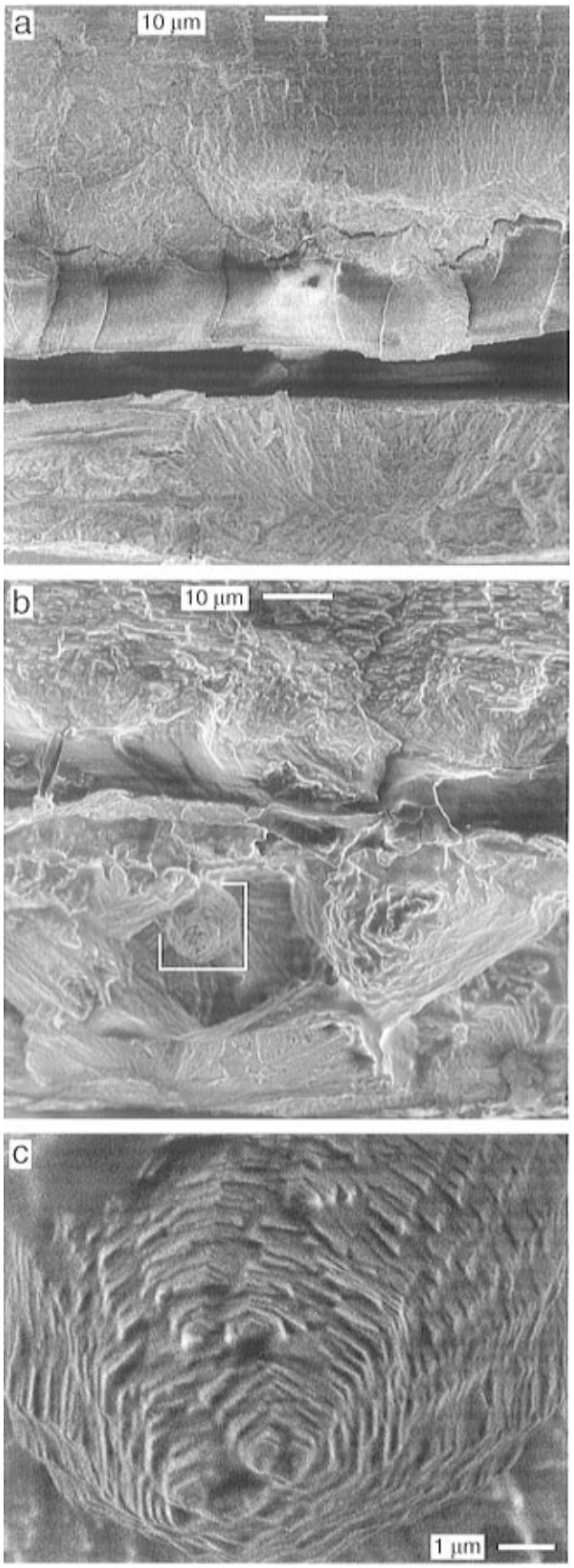

Figure 9. SEM images of vertical sections of flat pearls grown on (a) a roughened glass substrate and (b) a molybdenite substrate. In both, the growth direction is bottom to top. In (a), the horizontal black region is a gap created during sample handling and/or fracture. In (b), an aggregate of calcite crystallites whose growth directions are oriented nearly parallel to the substrate surface is in the lower right. (c) is an enlargement of the polycrystalline calcite aggregate delineated by the white square in (b).

(37) Manne, S.; Cleveland, J. P.; Gaub, H. E.; Stucky, G. D.; Hansma, P. K. *Langmuir* **1994**, *10*, 4409.

Discussion

Flat pearls are well-suited for this research because they provide ideal shell growth samples. Depending on both the location and duration of implantation in the animal, flat pearls comprise an array of different shell ultrastructures. Because the technique does not harm the animals, numerous growing flat pearls can be readily generated. This makes it possible to find samples that lack an organic cover masking the growth surface. It is therefore not necessary to pretreat samples, with either bleach[15,17,38] or cellulose acetate peels,[11] for high-resolution imaging of both organic and mineral features. Since growing flat pearls are thin, they can be readily viewed by transmission optical microscopy and easily fractured for vertical sections. Flat pearl nucleation and growth are sensitive to the chemical and physical properties of abiotic substrates. Finally, because the implanted substrates are flat, biomineral composites grown on them are flat as well and are therefore amenable to texture analysis by X-ray diffraction.

Flat pearls are useful analogues of the native shell. In both the shell and the flat pearl, nacre grows only on calcite surfaces. Two differently oriented calcite structures have been characterized. {10.4}-oriented calcite is deposited on both green and transparent organic sheets of flat pearls as well as on green organic sheets of native shell nacre. (00.1)-oriented calcite is deposited on both the distal edge of flat pearls and on the exterior side of the native shell. Both of these calcite structures contain elongated calcite crystallites of comparable dimensions with morphologies and growth directions (*c* axis) typical of geological calcite.

Biogenic calcite usually exhibits (00.1)-oriented nucleation.[39,40] The (00.1) calcite face is composed of either Ca^{2+} or CO_3^{2-} ions in a hexagonal array ($a = 4.99$ Å). The planes of the CO_3^{2-} ions are aligned with the (00.1) face. Nucleation from this face therefore meets stereochemical requirements for optimal coordination with an array of Ca^{2+} ions bound to organized acidic nucleation proteins.[40] Calcite crystallites on both the green and transparent organic sheets of flat pearls, however, exhibit {10.4}-oriented nucleation. Chicken eggshells comprise calcite spherulites with partial preferred {10.4} orientation.[41] This orientation, however, has not previously been reported in mollusc shells. The {10.4} calcite face is composed of both Ca^{2+} and CO_3^{2-} ions in two superimposed pseudohexagonal arrays ($a = 12.82$ Å, $\gamma = 101.9°$)[42] in which the planes of the CO_3^{2-} ions are inclined with respect to the crystal face. Since only one oxygen atom per CO_3^{2-} ion projects from the {10.4} face, this face is inadequate for optimal coordination with Ca^{2+} ions bound to acidic templating proteins. Nucleation from the {10.4} face is therefore an exception to the stereochemical requirement observed by Addadi and Weiner, which is consistently fulfilled by crystal nucleation in a wide range of biomineral systems.[40] The occurrence of {10.4}-oriented calcite in granular shells of foraminifera can be explained by a process in which crystals nucleate either in solution or nonspecifically on an organic matrix surface.[9] However, the unusually high degree of preferred {10.4} orientation (Figure 3a) of the densely packed, regularly inclined crystallites arranged in oriented aggregates on the transparent organic sheet (Figure 3) can be explained only by a well-controlled nucleation process. This process will be the subject of future investigations.

The aggregate crystallite structures of {10.4}-oriented calcite vary, depending on the type of organic sheet on which they are deposited. An approximately 140-nm-thick organic sheet deposited on glass favors the nucleation of a continuous layer of highly oriented polycrystalline aggregates (aggregate density ~350 mm^{-2}), as observed on the transparent organic sheet of growing flat pearls (Figure 3). In contrast, a 5−15-μm-thick bilayer organic sheet favors the nucleation of spherulites at discrete nucleation sites (nucleation density ~140 mm^{-2}), as observed on the green organic sheet of both flat pearls (Figure 4b) and native shell nacre (Figure 5b). In both cases, spherulite nucleation occurs on the spongy upper layer (OL2) rather than on the granular lower layer (OL1). On flat pearls, the location of the green organic sheet at the edges of substrates indicates that its deposition may be related to surface topology. Due to its thinness (140 nm), we have not detected the transparent organic sheet in the native shell. The blocklike calcite structure (found in the green organic/calcite heterolayer of native shell nacre) has been observed in flat pearls.

Green organic/calcite heterolayers of native shell nacre contain two calcite sublayers separated by a green organic sublayer (Figures 1a and 5b). High-calcium filaments span the organic sublayer and may maintain structural or mineralization continuity through the nacre. However, transorganic filaments are not necessary for nacre formation since nacre grows on both transparent-organic-sheet calcite of flat pearls and prismatic calcite of flat pearls and the native shell. In both cases, a green organic layer and the included calcium filaments are absent. The second calcite sublayer of the green organic/calcite heterolayer contains spherulites and is structurally analogous to that deposited on the flat-pearl green organic sheet (Figure 5).

Spherulitic crystallite aggregates are recognized components of mollusc shells. Spherulites form on the periostracum during early stages of prismatic calcite growth[13,43] and grow laterally until meeting to form oriented prisms.[13,21,43] Spherulites are also observed on organic material deposited on glass coverslips inserted between the mantle and the shell of bivalve molluscs (*Pinctada martensii*[23,26] and *Mytilus edulis*[26]) and in gastropod shell regeneration (*Helix pomatia*[44]). We now report that spherulitic calcite grows in the green organic/calcite heterolayers of red abalone nacre. In geology, calcite morphologies depend on the dissolved $[Ca^{2+}]/[CO_3^{2-}]$ ratio. The lower the ratio, the more elongated the crystallites.[32,34] Thus, spherulitic calcite comprising acicular crystallites forms under conditions of high carbonate supersaturation.[32,34] The more equant scalenohedron and prism morphologies result from relatively low carbonate concentrations.[34] Morphology is also influenced by crystal growth rate. The prismatic

(38) Bevelander, G. *Abalone: Gross and Fine Structure*; Boxwood: Pacific Grove, CA, 1988.
(39) Addadi, L.; Weiner, S. *Angew. Chem., Int. Ed. Engl.* **1992**, *31*, 153.
(40) Addadi, L.; Weiner, S. *Proc. Natl. Acad. Sci. U.S.A.* **1985**, *82*, 4110.
(41) Sharp, R. M.; Silyn-Roberts, H. *Biophys. J.* **1984**, *46*, 175.
(42) Ohnesorge, F.; Binnig, G. *Science* **1993**, *260*, 1451.
(43) Taylor, J. D.; Kennedy, W. J.; Hall, A. *Bull. Br. Mus. Nat. Hist. (Zool.) Suppl.* **1969**, *3*, 1.
(44) Abolins-Krogis, A. *Symp. Zool. Soc. London* **1968**, *22*, 75.

layer of mollusc shells, which originates from spherulites, is known to form rapidly in comparison with other shell ultrastructures.[45] In growing flat pearls, spherulitic calcite has a similarly rapid rate of growth, which is manifest in the poorly developed lateral walls of the crystallites. Therefore, in red abalone spherulitic calcite, horizontal striations and roughness along the crystallite long axes may result from intracrystalline protein occlusion, high carbonate supersaturation conditions, and/or rapid crystal growth rates.[32] Morphological variations may reflect relative differences in carbonate concentration.

The growth of flat pearls on roughened glass and molybdenite reveals that the implantation of substrates with physically and chemically perturbing properties may initially result in abnormal calcite deposition. On molybdenite, variations in the growth-direction orientations of the calcite crystallite aggregates, resulting from the interaction of biopolymers with the hydrophobic substrate surface, indicates that cooperative surface interactions play an important role in shell and flat pearl formation. The mollusc's generation of additional organic and calcite layers, with normal orientations, in response to these abnormalities reveals the animal's high level of control over the extracellular shell growth process. The "smart" response of the animal to the substrate is emphasized by the observation that the use of a previously formed flat pearl as a substrate does not result in the formation of an organic sheet and a calcite layer prior to nacre deposition.

The abrupt transition from the calcite phase to the nacreous aragonite phase which is observed (Figures 1, 5, 7, and 8a) has several remarkable features. The sharp phase-transition interface can be explained on a space−time basis which involves a growth inhibitor for calcite and/or a growth accelerator for aragonite. A precedent for this space−time control is seen in the abrupt transition, induced at metamorphosis, of the larval to the adult abalone shell. This transition is accompanied by a switch in production of the polyanionic proteins that control shell biomineralization.[7,8] Indeed, we have found in in vitro calcium carbonate growth experiments that a similarly abrupt calcite-to-aragonite transition is induced during the growth of calcite crystals by the addition of water-soluble, polyanionic proteins isolated from the aragonitic nacre of *Haliotis rufescens*. In these experiments, the crystallographic phases were identified by Raman microprobe spectroscopy (ν1(calcite) = 1086.2 cm^{-1}, ν4(calcite) = 712 cm^{-1}, ν1(aragonite) = 1083.5 cm^{-1}), and electron and X-ray diffraction.[35,46] The water-soluble, mineral-specific proteins used in these experiments were isolated and separated as described in ref 4. The implications of this biomolecular control of inorganic phase and growth dynamics are noteworthy and are being actively explored in our laboratories.[47]

Another notable aspect of the spherulitic-calcite-to-nacreous-aragonite transition is the rapid graded adjustment that is made in tablet thickness to quickly create a nacre ultrastructure which is strikingly flat. This adaptation is made for rough calcite layers with sharp protrusions as well as for more gently curved, undulating surfaces where peaks and valleys must be leveled off. This transition to a flat growth morphology is necessary to create the interlocking assembly of aragonite tablets that imparts nacre with its exceptional strength and fracture resistance.

Conclusion

This paper presents a comprehensive characterization of the structure, phase transitions, and growth processes of red abalone flat pearls. Spherulitic aggregates of {10.4}-oriented calcite crystallites in flat pearls are analogous to calcite spherulites in green organic/calcite heterolayers of native shell nacre. In contrast, prismatic calcite has preferred (00.1) orientation. Nucleation of highly {10.4}-oriented polycrystalline aggregates on the transparent organic sheet of flat pearls cannot be explained by typical stereochemical nucleation rationale. The calcite−aragonite transition is always abrupt, with the first aragonite crystals being either granular or tabular. We propose, as demonstrated by in vitro calcium carbonate growth experiments, that this transition is induced by water-soluble, mineral-specific, polyanionic biopolymers. Nacre deposition corrects for calcite surface roughness. Finally, the ability to grow nacre after irregular calcite growth on abnormal substrates reveals the adaptability of the multilayered biomineralization process. Our future work with red abalone shell formation will focus on its organic components. This will include investigating the process of {10.4}-oriented calcite nucleation on organic sheets, the role of the periostracum in prismatic calcite formation, and, particularly, the contribution of water-soluble polyanionic proteins and biomolecular processes to biomineralization.[35,46]

Acknowledgment. We thank William Wise for samples of molybdenite and for helpful discussions, Derron Walters, Robert Day, and Roberto Gonzalez-Plaza for helpful discussions, Neal Hooker and Hoa Bui for flat pearl production, Anna Davis for Feigl staining experimentation, Mark Cornish and Matthew Lefevre for SEM assistance, and D. J. McLaren and Anne Marie Kral for production of the figures. This work was supported by the Biosciences and Materials Research Divisions of the National Science Foundation under award MCB-9202775 (P.K.H., D.E.M., G.D.S., C.M.Z.), the MRL Program of the National Science Foundation under Award DMR-9123048 (A.M.B., P.K.H., Y.L., D.E.M., J.S.S., G.D.S.), the Office of Naval Research under award N00014-93-1-0584 (A.M.B., P.K.H., D.E.M., G.D.S.), Grant R/MP-65 from the U.S. Dept. of Commerce (NOAA)−California Sea Grant College Program (P.K.H., D.E.M., G.D.S., C.M.Z.), and a fellowship from the Deutsche Forschungsgemeinschaft (M.F.). This work made use of MRL Central Facilities supported by the National Science Foundation under Award No. DMR-9123048.

CM9503285

(45) Currey, J. D. *J. Mater. Ed.* **1987**, *9*, 118.

(46) Morse, D. E.; Gonzalez-Plaza, R.; Belcher, A. M.; Zaremba, C.; Stucky, G. D.; Fritz, M.; Walters, D.; Hansma, P. K.; Speck, J.; Mann, S. *Proteins and Mechanisms Organizing Biomineralization to Form the Microlaminate Components of Abalone Shell*; IV International Conference on Advanced Materials, Aug 27, 1995.

(47) Note added in proof: We recently learned that similar results on polymorph selection have been obtained independently by researchers at the Weizmann Institute, using proteins from the shells of other molluscs and a heterologous substrate: Falini, G.; Albeck, S.; Weiner, S.; Addadi, L. *Science* **1996**, *271*, 67.